Journal of Molecular Structure 1252 (2022) 132093

Contents lists available at ScienceDirect

Journal of Molecular Structure

journal homepage: www.elsevier.com/locate/molstr

Fischer carbene complexes of cobalt(I): Synthesis and structure

Mmushi M. Moeng[a], Frederick P. Malan[a], Simon Lotz[a], Daniela I. Bezuidenhout[b,*]

[a] Department of Chemistry, University of Pretoria, Private Bag X20, Hatfield 0028, Pretoria, South Africa
[b] Laboratory of Inorganic Chemistry, Environmental and Chemical Engineering, University of Oulu, P.O. Box 3000, 90014 Oulu, Finland

ARTICLE INFO

Article history:
Received 29 October 2021
Revised 2 December 2021
Accepted 3 December 2021
Available online 5 December 2021

Keywords:
Fischer carbene
Cobalt carbonyl
Carbene complex substituents
Aminocarbene
Alkoxycarbene

ABSTRACT

Three different aryl substrates thiophene (ThH), ferrocene (FcH) and *p*-bromodimethylaniline (*p*-DMABr) were lithiated and reacted with $[Co(CO)_4SnPh_3]$, according to the Fischer carbene protocol. The products $[CoSnPh_3(CO)_3\{C(OEt)R\}]$ (*R* =Th, **1**, *p*-DMA, **2** and *R* = Fc, **3**) were analysed to unravel the role of the aryl carbene substituent in stabilizing intermediates and final products. The ethoxy carbene complexes were aminolysed by *in situ* generated $HNMe_2$ to afford $[CoSnPh_3(CO)_3\{C(NMe_2)R\}]$ (*R* =Th, **4**, *p*-DMA, **5**) and with *N,N*-dimethylethylenediamine $[CoSnPh_3(CO)_3\{C(NHCH_2CH_2NMe_2)R\}]$ (*R* = *p*-DMA, **6**) in high yields. The trigonal $Co(CO)_3$ in the equatorial plane is very stable and efforts to displace a carbonyl in **6** was unsuccessful, both by heating and irradiation. The role of the aryl carbene substituents in stabilizing the electrophilic carbene carbon was investigated and studied by NMR spectroscopy in solution and single crystal X-ray structure determinations.

1. Introduction

Inexpensive and earth-abundant first row transition metal complexes with N-heterocyclic carbene (NHC) ligands have proved attractive and viable alternatives to their 4*d* and 5*d* transition metal counterparts as, for example, homogeneous catalysts over the past two decades [1–4]. Examples of acyclic Fischer-type [5] carbene complexes of 3*d* metals in this context are virtually unknown. As a continuation of our interest in preparing catalytically-relevant Fischer carbene complexes of the late transition metals [6–8], the synthesis of a model series of cobalt(I) carbonyl Fischer carbene complexes (FCCs) with varying heteroatom- and (hetero)aryl carbene substituents is reported herein.

The first reports detailing the preparation of cobalt(I) FCCs involved nucleophilic attack of cobalt carbonyl precursors stabilized by triphenylstannyl, -germyl or -plumbyl ligands, to yield complexes of the type $[Co(CO)_3(YPh_3)\{C(OR)R'\}]$ (*Y* = Sn, Ge, Pb; *R* = Et, Me and R′= Me, Et, *n*-Pr, *n*-Bu, Ph) [9–13]. Hence, in the synthesis of Co(I) FCCs, the imperative of effective nucleophilic carbonyl attack needs to be facilitated by a bulky ancillary ligand on the cobalt precursor to electronically and structurally direct and stabilize acyl formation. The intermediate acylate stabilization is required for successful alkylation to generate neutral FCCs. In practise this means that for more basic metals, metal alkylation competes with *O*-alkylation, as is well documented for iron(0) acylates [9,14–18]. As a result, the number of examples of Co(I) FCCs available from the classic Fischer route is very limited. A prerequisite towards stable FCCs of cobalt(I) is therefore carbene substituents with steric and electronic properties that allow for fine tuning of electron delocalization during the formation of the acylate intermediate and the final FCC. The aim of this study was to evaluate the possibility of using different, more flexible, π-electron excessive aryl substituents and study their role to effectively facilitate the stabilization of electrophilic Fischer carbene (FC) carbon atoms. These include 2-thienyl (Th) [19–22], *N,N*-dimethylaniline (*p*-DMA) [23,24] and ferrocenyl (Fc) [19,25], which have very different features for either π-delocalization and/or σ-inductive effects (Fig. 1) [26]. Comparison of NMR spectroscopic data in solution with solid state crystal structural data is relevant in this study to correlate electronic and structural properties.

2. Results and discussion

2.1. Synthesis and spectroscopic characterisation of cobalt(I) FCCs

No prior records were found for cobalt(I) FCCs with thienyl (Th), *p*-*N,N*-dimethylaniline (*p*-DMA) or ferrocenyl (Fc) substituents. Optimum conditions for lithiations of *p*-DMA-Br entail lithium-bromine exchange reaction with *n*-BuLi in THF at low temperatures [27–29]. Higher yields of the *p*-lithiated DMA were obtainable by using diethyl ether instead of THF. Thiophene (ThH) was lithiated in THF, and even though dilithiation can also occur

* Corresponding author.
E-mail address: daniela.bezuidenhout@oulu.fi (D.I. Bezuidenhout).

https://doi.org/10.1016/j.molstruc.2021.132093

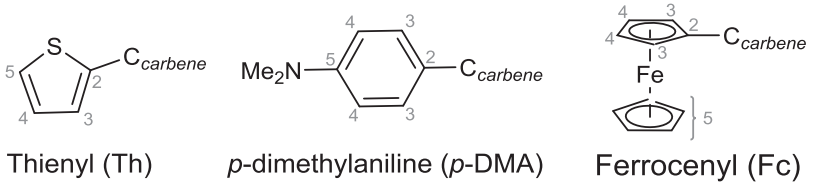

Fig. 1. Fischer carbene aryl substituents with atom numbering.

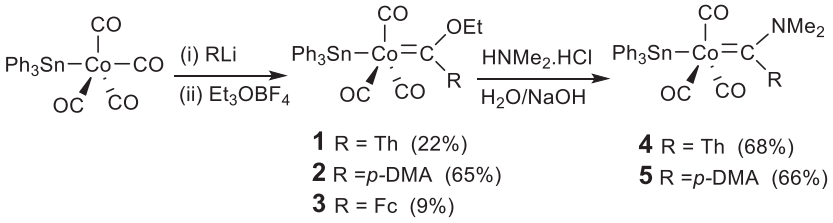

Scheme 1. Synthesis of Co(I) FCCs **1**–**5**.

when deprotonating at low temperature [19], no biscarbene complexes were isolated. To avoid dilithiation of ferrocene, *tert*–BuLi is used instead of *n*-BuLi [30]. The classic Fischer route was used to prepare the ethoxycarbene complexes (FCCs) **1**–**3** (Scheme 1) [5]. The incorporation of $SnPh_3$ in the cobalt(I) carbonyl precursor $[Co(CO)_4(SnPh_3)]$ [31] has steric and electronic advantages during nucleophilic attack on the otherwise more labile carbonyl ligands. This is essential for the progress of the reaction during the formation of the acylate intermediate and successful alkylation with Meerwein's salt [32] in dichloromethane afterwards. The ratio of heteroaromatic precursor and excess lithiating agent used during the reactions for the different reagents was experimentally optimized to give the maximum yield of the corresponding Fischer monocarbene complex. Challenges initially experienced during the syntheses are the insolubility of the metal carbonyl precursor during the nucleophilic attack step at low reaction temperatures (−78 °C) and later excessive decomposition during the purification of the FCCs. The yields of the cobalt(I) FCCs vary from very low (Fc, 9%), to low (Th, 22%) and very good for *p*-DMA (65%). We ascribe the relative high yield of **2** to the presence of the distant *p*-NMe_2 donor group that acts as a tunable electronic switch during ligand modifications (*vide infra*). Recent studies have shown that in both W- [23] and Pt-FCC [24] containing a *p*-DMA carbene substituent, the remote NMe_2 facilitates electronic stabilization of the carbene ligand. The orange (**1**) to red solids (**3**) are relatively stable although they were handled under inert conditions. With the exception of **3**, the complexes can be readily crystallized from saturated solutions of dichloromethane (DCM).

Ethoxycarbene complexes have enhanced electrophilicity at the carbene carbon atom because of the high electronegativity of the oxygen atom and are readily aminolysed by a nucleophilic substitution reaction of a strong secondary amine donor. Aminolysis of **1** and **2** is achieved by the reaction of the ethoxycarbene complexes with the *in situ* generated dimethylamine [33]. The latter was obtained after reacting dimethylammonium chloride in THF with an aqueous base (NaOH). The reaction mixture of either **1** or **2** and $NHMe_2$ was stirred vigorously until the carbene complex was completely converted as was indicated by thin layer chromatography (TLC). The orange-red solution gradually becomes lighter and eventually the aminolysed FCCs are isolated from a light yellow solution. Unlike for **1** (Th) and **2** (*p*-DMA) which afforded **4** (68%) and **5** (66%), respectively, all attempts to aminolyse **3** failed. A possible explanation is found in excessive decomposition of **3** whereby unwanted redox reactions play an important role. Electrochemical studies have revealed that the ferrocenyl unit contribution to stabilization of the [M]=C centre is comparable to that of the NHR moiety [19].

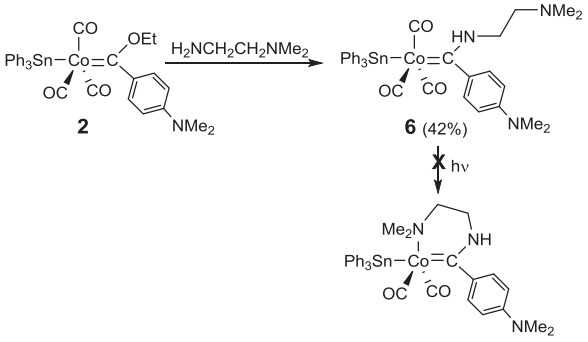

Scheme 2. Aminolysis of **2** with *N,N*-dimethylethylenediamine.

In a control experiment, **2** was successfully aminolysed with *N,N*-dimethylethylenediamine to afford **6** (42%). The aminocarbene is ideally suited to form a six-membered chelate ring by the substitution of a carbonyl ligand by the distant dimethylamino group (Scheme 2). By applying harsh reaction conditions like refluxing the reaction mixture or by irradiation of a hexane/thf (10:1) mixture, no carbonyl substitution was evident and decomposition resulted. It is anticipated that substitution of a carbonyl ligand from the very stable tricarbonyl equatorial plane requires too much energy to retain carbene complex stability.

2.2. NMR spectroscopy

The ^1H and ^{13}C NMR chemical shifts of selected atoms are summarised in Table 1. The same atom numbering system as, indicated in Fig. 1, is used, and the spectra of **1**–**6** are provided in the ESI. In $[Co(SnPh_3)(CO)_4]$ the chemical shifts of the phenyl protons (7.33 ppm) are *ca* 0.3 ppm upfield from the corresponding protons of the tin ligand in the FCCs **1**–**3.** This is best recognizable in the well-resolved *o*-proton, not affected by overlapping of *m-p* resonances or tin satellites and resonate at 7.61–7.67 ppm as high intensity peaks in **1**–**6**. The Ph-signals of the aminolysed carbene complexes are slightly upfield compared to analogous signals of the ethoxycarbene complexes. This is in line with the bonding properties of amino *vs* ethoxy substituents in FCCs. Although a small effect, the upfield shifts implies less transfer of electron density from $SnPh_3$ ligand *via* the Co to the *trans* carbene carbon.

In Fig. 2 the chemical shifts of the aryl protons of ThH, DMAH and FcH are compared with the corresponding shifts of these sub-

Table 1
Selected NMR spectral data (δ, ppm; J, Hz) for the FCCs **1–6** in solvent $CDCl_3$.

^{1}H NMR	1	2	3	4	5	6	^{13}C NMR	1	2	3	4	5	6
H3	8.31, 1H, dd (4.0, 1.0)	7.97, 2H, d (8.8)	5.10, 2H, s	7.33, 1H, br (dd)	6.80, 2H, d (8.7)	7.11, 2H, d (8.8)	C_{carb}[a]	297.0	304.1	309.5	252.2	257.9	258.5
H4	7.20, 1H, dd (4.9, 4.1)	6.61, 2H, d (8.9)	4.81, 2H, s	7.00, 1H, dd (5.0, 3.5)	6.70, 2H, d (8.7)	6.70, 2H, d (8.8)	CO	200.7	200.8	201.1	200.0	200.3	201.7
H5	7.83, 1H, dd (4.0, 1.0)			6.64 1H, dd (3.5, 1.1)			C2[a]	154.7	154.2	74.7	152.0	148.9	150.3
$C_{carb}O-CH_2$	5.07, 2H, q (7.1)	5.07, 2H, q (6.9)	4.97, 2H, q, (7.1)				C3	140.8	132.9	72.7	127.0	122.1	125.2
CH_3	1.69 3H, t (7.1)	1.68, 3H, t (7.0)	1.64, 3H, t, (7.1)				C4	129.0	110.4	69.7	119.8	111.5	110.9
Cp			4.26, 5H, s				C5	137.0	139.4	70.9	124.9	141.5	136.1
CH_2-CH_2						3.44, 2H, q (11.3, 5.4); 2.47 2H, t (11.7, 5.7)	OCH_2CH_3	77.7, 14.7	77.7, 14.9	77.7, 14.9			
$C_{carb}N(CH_3)_2$				4.00, 3H, s; 3.34, 3H, s	3.97, 3H, s; 3.22, 3H, s		$C_{carb}-N-(CH_3)_2$				51.1, 45.9	50.6, 45.3	
$N-(CH_3)_2$		3.11, 6H, s			2.97, 6H, s	3.02, 6H, s; 2.30, 6H, s	$N-(CH_3)_2$		40.1			40.2	45.1, 40.2
NH						9.59, 1H, s (br)	CH_2-CH_2						57.2, 47.7

[a] C1 is the carbene carbon and C2 the *ipso* carbon of the aryl substituent.

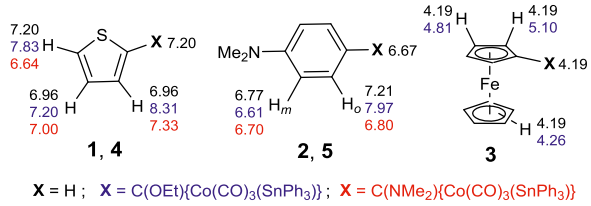

Fig. 2. ^{1}H NMR chemical shifts (ppm) of RH (R = Th, *p*-DMA and Fc) [28,29,34] and FCCs **1–5**.

stituents in the ethoxy- and aminocarbene ligands of complexes **1–5** [28,29,34]. Correlation between the differences in shifts and electronic implications of carbene ligands in the complexes is investigated. The different proton chemical shifts, for protons in α-, β-, etc. positions with respect to the carbene site, are indicated for all ring protons in Fig. 2. The chemical shifts of the protons of the aryl substituent closest (α) to the carbene carbon are the most affected, while all ring protons of aryl substituents are connected *via* a π-conjugated pathway with the strong electron withdrawing carbene carbon. The differences of the chemical shifts ($\Delta\delta$, ppm) between RH and [Co{$SnPh_3$}$(CO)_3${C(OEt)R}] for the complexes **1–3** (R = Th, *p*-DMA and Fc) follow the order for the α-protons: Th (**1**, $\Delta\delta$ 1.35) > Fc (**3**, $\Delta\delta$ 0.91) > DMA (**2**, $\Delta\delta$ 0.76). Compared to a proton in the aryl substrate, the carbene carbon in the complexes drains electron density from all the rings. We ascribe the reason why *p*-DMA is more shielded to the π-mesomeric delocalization effect of electron density transferred towards the carbene carbon by the remote, external NMe_2 moiety. Stabilization of FCCs by heteroaryl rings or remote *p*-nitrogen substituents in conjugated rings are under explored [35,36]. Confirmation of a strong electron transfer effect by the remote NMe_2 is also found in the chemical shifts of the β-protons which are more shielded for DMA (Fc ($\Delta\delta$ 0.62) > Th ($\Delta\delta$ 0.24) > DMA ($\Delta\delta$ −0.16)).

Stabilization of the FC carbon of Th and Fc substituents is furthermore evident from H5 ($\Delta\delta$, ppm) in Th which is 0.63 ppm downfield compared to ThH. Both protons of the Cp-ring attached to the carbene carbon in Fc, is moved downfield compared to FcH (4.19 ppm) and emphasises the movement of electron density towards the carbene carbon [34]. In Fc the two α-protons (H3) adjacent to the carbene carbon appear as a single peak more downfield at 5.10 ppm with the β-protons (H4) at 4.81 ppm, while the five protons of the other free rotating Cp-ring display a single peak at 4.26 ppm. Unlike for the aminocarbene complexes (**4–6**), the ethoxy substituent in **1–3** is generally not very effective in stabilizing the electron withdrawing carbene carbon. In **4–6** the amine substituent of the aminocarbene displays chemical shift differences for the α-protons: Th (**4**, $\Delta\delta$ 0.37) > *p*-DMA (**5**, $\Delta\delta$ −0.41), (**6**, $\Delta\delta$ −0.10). In this instance the aminocarbene substituents play the major role in stabilizing the carbene carbon, while the role of the aryl substituents is less pronounced.

Fig. 3 shows the stacked ^{1}H NMR spectra of **2** and **5.** Comparison of the chemical shifts of *p*-DMAH with **2** and **5** for the *ortho*-H and *meta*-H protons of the DMA substituent in the ethoxy *vs* aminocarbene displays the trend ($\Delta\delta$: Δ= H_o - H_m, ppm): **2** ($\Delta\delta$ 1.36) > *p*-DMAH ($\Delta\delta$ 0.44) > **5** ($\Delta\delta$ 0.10). The data reveal that the polarization between H_o and H_m protons in the aryl ring is unambiguously significant for **2** and separates the benzene ring into two fragments, an electron rich (shielded) segment {$Me_2N-C(CH_m)_2$} and an electron poor (deshielded) segment {$C_{carb}-C(CH_o)_2$}. This we ascribe to the shift of electron density from the remote nitrogen to the benzene ring. A similar polarization in *p*-DMAH and **5** is small, with the smallest difference observed for **5**. The large difference between the chemical shifts of H_o and H_m for *p*-DMA in the complexes are clearly indicated in the ^{1}H NMR spectra of **2** and **5.**

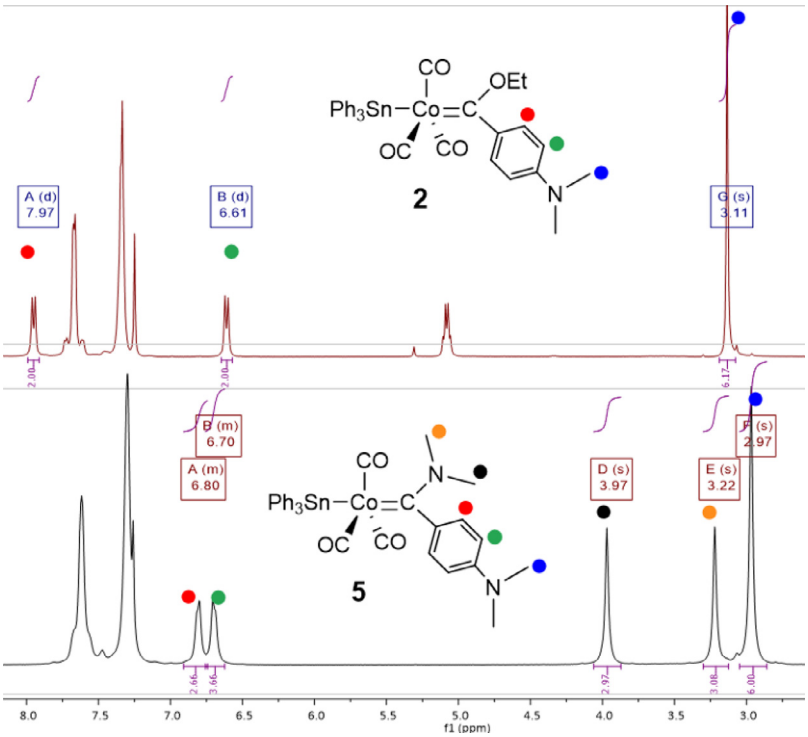

Fig. 3. Stacked ^{1}H NMR spectra (selected region) of **2** (top) and **5** (bottom).

On moving from **2** to **5** the H_o signal moves from 7.97 to 6.80 ppm upfield while the downfield shift of H_m (6.61 to 6.70 ppm) is very small. Unlike in **2**, the distant, remote NMe_2-substituent of DMA in **5** does not play a significant role.

Secondly, the distant NMe_2 resonance in *p*-DMAH is a singlet at 2.89 ppm, which is shifted downfield in **2** (3.11 ppm) also indicating electron transfer from the remote NMe_2 moiety *via* the phenyl ring towards the electron withdrawing carbene carbon. By contrast the corresponding resonance in **5** is upfield (2.97 ppm), indicating a smaller donor involvement of the remote NMe_2 moiety in this case. The predominant stabilization of the carbene carbon is now effected by the aminocarbene substituent which is adjacent to the carbene carbon. The C_{carb}–N bond order is high and restricting rotation places the two Me groups in different electronic environments at 3.97 and 3.22 ppm. The *anti*/*E*-methyl is shifted more upfield at 3.22 ppm compared to the *syn*/*Z*-substituent methyl [37–39].

In the ^{13}C NMR spectra (ESI) the carbene carbon resonates at *ca.* 40 to 50 ppm upfield in the aminocarbene complexes (**4**–**6**) compared to their ethoxycarbene analogues (**1**–**3**), highlighting the dominant bonding interaction of the attached nitrogen in the aminocarbene compared to an ethoxy-oxygen with the electron poor carbene carbon. The carbene carbon chemical shifts (ppm) follow the order Fc (**3**, δ 309.5) > *p*-DMA (**2**, δ 304.1 > Th (**1**, δ 297.0) >> *p*-DMA (**6** and **5**, δ 258.5 and δ 257.9) > Th (**4**, δ 252.2). The carbonyl chemical shifts appear as a single peak around 201 ppm (200.0–201.7 ppm) in the spectra of all FCCs (**1**–**6**). Hence the carbonyl resonances are not affected by the different carbene substituents and electronic effects affect mostly the ligands in the axial positions of the trigonal bipyramidal structure. The trigonal planar equatorial carbonyls form the core of the complexes and we ascribe the stability of the FCCs **1**–**6** to the presence of the three equatorial carbonyl ligands. The polarization effect of the alkoxy carbene substituent and concomitant remote amine-mediated stabilization of **2** and **5**, in combination with cobalt carbonyl core stabilization on the carbene moiety, are highlighted when the NMR chemical shifts of the H_o proton and C_{carb} atom for different *p*-DMA-substituted metal carbene complexes are compared (Fig. S13, ESI). H_m proton resonances are mostly unaffected, while the different complex composition accounts for the shielding of the FC carbon in the ^{13}C spectrum of the platinum(II) carbene complexes [24], compared to the negligible differences observed in the H_o /C_{carb} resonances of the previously reported tungsten [23] and cobalt carbonyl complexes **2** and **5**.

The resonance structures depicted in Fig. 4 represent the potential role played by the $Co(CO)_3SnPh_3$ fragment to stabilize the electropositive FC carbon (**A**). The moving of electron density towards the carbene carbon by π-donation along a conjugated pathway and subsequent stabilization of the carbene carbon and the complex are illustrated with **B** and **C**. The two zwitterionic structures could be meaningful descriptors originating from contributions by the carbene substituents, the thienyl ring (**B**) and/or the heteroatom substituent (**C**). The NMR data suggests that a meaningful contribution of resonance structure **B** is evident in the ethoxycarbene complex while a greater contribution of the structure **C** is indicated in the aminolized complex.

2.3. Infrared spectroscopy

The infrared spectroscopic data of complexes **1**–**6** are summarised in Table 2. In **1**–**6**, the FCCs $Co(CO)_3L_2$ with the three carbonyls in the trigonal equatorial plane and the two unique ligands in axial positions, display D_{3h} symmetry with stretching vibrational modes and assignments as listed in Table 2 [9–13]. The three carbonyls in the equatorial plane display a broad high intensity band at lower frequency, assigned to the E-mode. A weak satellite band appears at higher frequency resulting from equatorial symmetric C–O stretches assigned to the formally infrared inactive $A_1^{(1)}$ mode, and becomes active due to vibrational couplings. This was not observed for the ferrocenyl substituent. The appearance of the $A_1^{(1)}$ vibrational bands in these complexes indicates that the three carbonyl ligands are affected and becomes slightly non-coplanar in arrangement due to the steric effect arising from the $SnPh_3$ and carbene ligands. The strong E-band indicates that

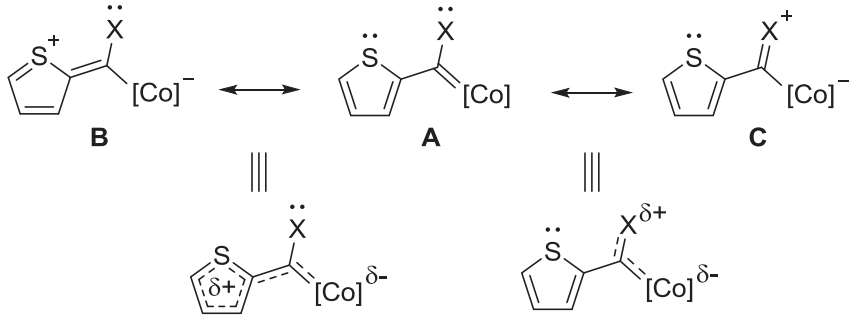

Fig. 4. Most important resonance structures relevant in the thienylcarbene ligand.

Table 2
Carbonyl stretching vibrational frequencies (ν_{CO}, cm^{-1}) of **1**–**6**.

Mode	1	2	3	4	5	6
$A_1^{(1)}$	2033 vw	2016 vw	n.o.	2020 vw	2016 vw	2011 vw
E	1955 s	1945 s	1946 s	1952, 1937 s	1956, 1937 s	1939 s

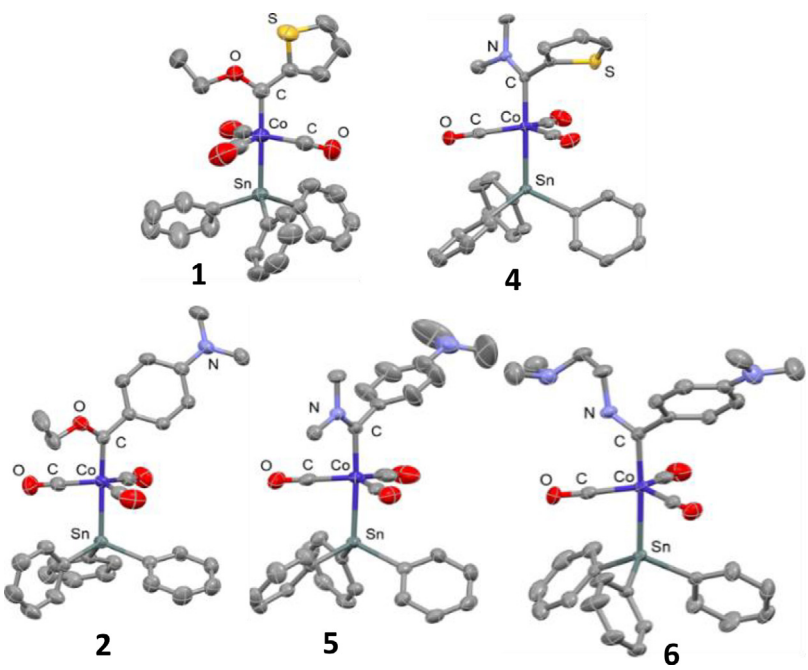

Fig. 5. Molecular structures of **1, 2, 4**–**6**. Hydrogen atoms were omitted for clarity. Atomic displacement ellipsoids are shown at the 50% probability level. For **5**, a molecule of $CDCl_3$ have been omitted for clarity.

the three carbonyl bands are symmetrically arranged in the equatorial plane of the trigonal-bipyramidal complexes. However, the asymmetry and bulk of the carbene and $SnPh_3$ ligand in the axial positions may lead to a splitting of the E-band into two non-degenerate bands. Steric effects, as well as favourable electronic effects in **4** and **5,** place the aminocarbene substituent (NMe_2) in the plane of the carbene ligand, resulting in crowding and small deviations within the equatorial plane leading to E-band splitting or broadening.

2.4. Single crystal X-ray molecular structures

Crystallization of **1, 2** and **4**–**6** was done by layering saturated DCM solutions of the FCCs with hexane. Single crystal X-ray diffraction studies confirm that the five Co(I) structures display a trigonal bipyramidal molecular arrangement of ligands with the three carbonyl ligands in the equatorial plane and the FC carbon and $SnPh_3$ ligands in the two axial positions (Fig. 5). Unfortunately, isolation of single crystals for solid state structure studies of the ferrocenyl FCC of cobalt(I) could not be accomplished.

Selected bond lengths, angles, torsion angles and appropriate planes are given in Table 3. The structures display minor deviation both in the equatorial plane and along the axial axis from ideal trigonal bipyramidal symmetry. In **1** the sulphur atom of the thienyl substituent is *cis* to the oxygen atom of the ethoxy substituent, Fig. 5 [40–42]. Due to restricted ring rotation around the C_{carb}–C_{ipso}(Th) bond in **4** the sulphur atom is found in either of two possible positions of the thiophene ring and is accounted for by refining the structure with weighted positional fractions.

The equatorial plane is described by the three carbonyl ligands in the centre of the molecule. A plane P1 (O1–O2–O3) in the equatorial region touching the three oxygen atoms of the three carbonyl ligands with respect to the position of the Co atom, is investigated. Angular views of the P1 plane in the molecules are shown in Fig. 6. Plane P1 bisects the axial axis and shortens the Co–Sn bond by 0.387(3) Å in **1**, indicating an umbrella formation

Table 3
Selected bond lengths (Å), bond angles (°) and torsion angles (°) of the structures **1**–**6**.

Bond lengths (Å)	**1**	**4**	**2**	**5**	**6**
Co–C_{carb}	1.913(3)	1.953(2)	1.922(2)	1.953(4)	1.948(2)
Co–Sn	2.5688(5)	2.545(1)	2.560(9)	2.530(1)	2.541(1)
Co–C(O)	1.771(4), 1.763(4), 1.781(4)	1.759(2), 1.790(2), 1.770(2)	1.760(2), 1.785(2), 1.772(2)	1.771(6), 1.772(5), 1.787(6)	1.757.(2), 1.768(2), 1.796(3)
C_{carb}–C2/C_{ipso}	1.443(4)	1.479(3)	1.456(3)	1.483(6)	1.470(3)
C_{carb}–$X_{O/N}$[a]	1.318(4)	1.307(2)	1.319(2)	1.296(6)	1.312(3)
C2/C_{ipso} –C3	1.363(5)	1.403(11)[b], 1.356(9)[b]	1.401(3), 1.401(3)	1.361(8), 1.361(8)	1.393(3), 1.401(3)
C3–C4	1.396(6)	1.589(12)[b],1.588(12)[b]	1.367(3), 1.371(3)	1.394(1), 1.396(9)	1.378(4), 1.372(4)
C4–C5	1.336(7)	1.325(6)[b], 1.325(6)[b]	1.407(3), 1.407(3)	1.362(1), 1.367(1)	1.401(4), 1.398(4)
N2–C5			1.360(2)	1.431(7)	1.370(3)
Bond angles (°)	**1**	**4**	**2**	**5**	**6**
C2/C_{ipso}–C_{Carb}–$X_{O/N}$	107.3(3)	115.6(2)	108.4(2)	115.7(4)	116.1(2)
C2/C_{ipso}–C_{Carb}–Co	126.2(2)	117.4(1)	125.6(4)	117.9(3)	123.2(2)
Co–C_{Carb}–$X_{O/N}$	126.5(5)	127.0(2)	125.9(1)	126.4(3)	120.7(2)
Sn–Co–C_{carb}	177.7(10)	175.3(1)	171.4(1)	174.4(7)	176.9(1)
Sn–Co–$C(O)_{av}$	82.5(3)	84.9(3)	84.1(3)	84.8(4)	84.9(1)
C_{carb}–Co–$C(O)_{av}$	97.6(3)	95.1(3)	96.3(3)	95.2(7)	95.1(1)
(O)C–Co–C(O)	112.8(2), 120.9(2), 121.2(2)	122.3(1), 117.4(1), 117.9(1)	109.6(2), 120.5(1), 126.5(3)	116.7(3), 117.7(3), 123.1(2)	117.5(1), 118.9(1), 121.3(1)
Torsion angles (°)	**1**	**4**	**2**	**5**	**6**
Co–C_{carb}–C2–C3	21.1(6)	−104.1(7)	−29.6(3)	−119.6(7)	57.5(3)
$X_{O/N}$ –C_{carb}–C2–C3	−159.6(4)	77.8(9)	149.3(8)	61.6(9)	56.3(3)
C_{het}[c]– $X_{O/N}$ –C_{carb}–Co	−4.8(5)	−179.4(1), 4.0(3)	5.1(8)	7.0(6)	−175.4(2)
H_3C–N2–C2–C3			−5.1(3)	−5.1(9)	−2.5(4)
OC[d]–Co–C_{carb}–$X_{O/N}$	−48.2(0), 75.4(5), −161.2(7)	−51.2(2), 71.4(2), −171.0(2)	47.7, −81.0(9), 157.5(2)	−177.9(5), 63.3(8), −62.5(5)	84.3(8), −156.8(5), 145.2(3)
OC[e]–Co–Sn–C2	−48.4(9), 75.1(8), −160.9(8)	−51.2(2), 71.4(4), −177.9(5),	−58.2(5), 71.7(9), −166.2(6)	−50.4(9), −67.7(7), 177.1(7)	−74.0(5), 46.2(3), 167.6(4)
Planes (Å)	**1**	**4**	**2**	**5**	**6**
P1[f]–Co	0.387	0.236	0.292	0.257	0.241
P2[g]–C2	0.015	0.047	0.025	0.053	0.072
P3[h]–$X_{O/N}$	0.014	0.037	0.022	0.042	0.066

[a] $X_{O/N}$: O represents OEt and N is NMe_2.
[b] Distances affected because sulphur are found in both S and C3 sites in the molecule.
[c] C_{het}: represents the carbon atom adjacent to $X_{O/N}$.
[d] Shows the rotation sites of the three carbonyls around the Co–C_{carb} bond with respect to X.
[e] Defines orientation of one CO with respect to the three phenyl *ipso*-carbons of Sn (Co–Sn bond rotation).
[f] Plane defined by the three oxygen atoms of the carbonyl ligands.
[g] Plane defined by $X_{O/N}$–C_{carb}–Co.
[h] Plane defined by C2–Co. C2 = C_{ipso}.

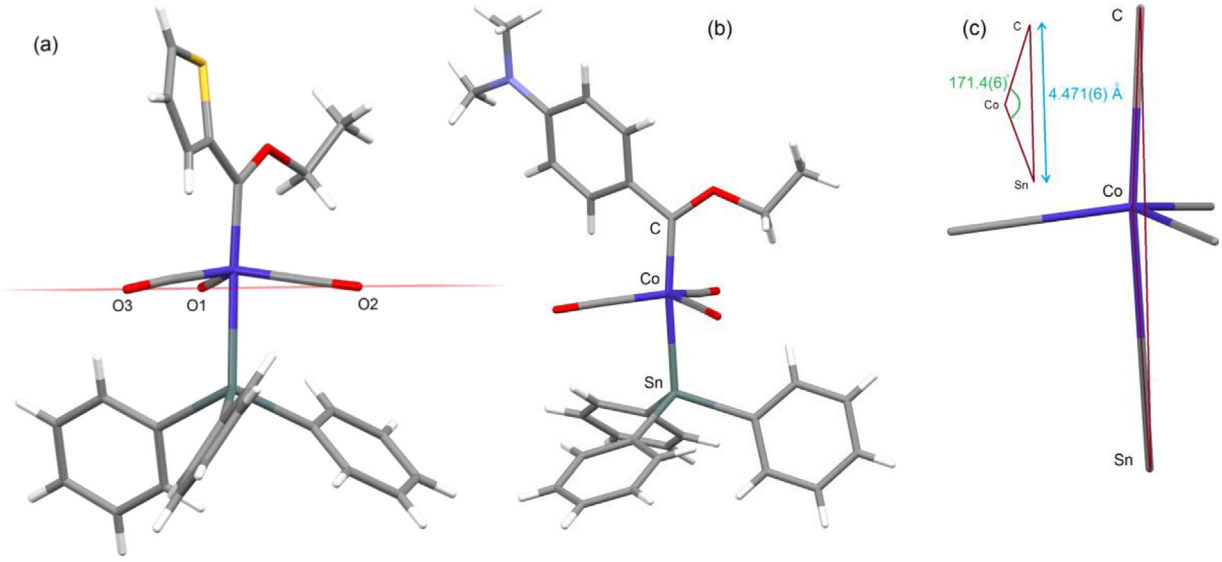

Fig. 6. Capped sticks model of **1** with a mean plane (P1) through the carbonyl oxygens in the equatorial plane showing Co(I) distortions in the plane (a); Capped sticks model of **2** showing the deviation from the axial axis (b, c).

of three carbonyls on top of a plane with Co at the apex [43]. Displacement along the axial axis relative to P1 are: 0.387 Å (**1**) and 0.236 Å (**4**) for the Th-carbene complexes and 0.292 Å (**2**) > 0.257 Å (**5**) > 0.241 Å (**6**) for the *p*-DMA complexes. This is also confirmed by bond angles (Sn–Co–$C(O)_{av}$) smaller than 90° and (C_{carb}–Co–$C(O)_{av}$) greater than 90°, Table 3. In both Th and *p*-DMA complexes, the largest displacement from Co along the axial axis relative to P1 is observed for the ethoxycarbene complexes. The less bulky ligand in **1** displays an even greater deviation compared to **2.** The distance from Sn to C_{carb} is 4.481(8) Å in **1**, while the Co–C_{carb} and Co–Sn bond lengths are 1.913(3) Å and 2.569(1) Å respectively, indicating that the centroid of this complex is underneath the umbrella. A similar observation as in **1** is recorded for other complexes investigated, **2, 5** and **6**. Support for this argu-

ment is found in a decreasing Co–C_{carb} bond distance of the FCCs in the same order (Å): **4** (1.953(2)) ≈ **5** (1.953(4)) > **6** (1.948(2)) > **2** (1.922(2)) > **1** (1.913(3)). The poorer π-donor contribution of an ethoxy substituent compared to an amino substituent is compensated for by the cobalt fragment. As a result, a greater involvement of Co is seen for π-interaction with the carbene carbon in **1** and **2** compared to **4, 5** and **6**.

The angle Sn–Co–C_{carb} of the five complexes **1, 2, 4, 5** and **6** at 177.7(1)°, 171.4(6)°, 175.4(6)°, 174.4(7)° and 176.9(1)°, respectively indicates that the cobalt atom is slightly displaced along the axial axis from ideal trigonal bipyramidal symmetry. The deviation is shown in Fig. 6. The greatest deviation (*ca.* 9°) is found for **2** and the smallest for **1**, both ethoxycarbene complexes. The ethoxy and the amino carbene substituents occupy positions opposite the space of two equatorial carbonyl ligands and is approximately in a staggered conformation with two carbonyl ligands in the middle of the molecule (Fig. 6). By contrast, the aromatic ring substituent is more or less in an eclipsed conformation with the third carbonyl ligand. The two axial ligands are bent towards the open space between the two carbonyls and away from the linear axial axis defined by C_{carb}–Sn [43]. Similar to the carbonyls, the tin phenyl substituents form an umbrella with the benzene rings tilted and orientated to be opposite to the open spaces between the carbonyl ligands. As a result, the ethoxy or amino substituent is in an eclipsed conformation with one of the Sn phenyls.

Thiophene is an electron excessive planar molecule and a potential π-electron donor *via* a conjugated pathway from the sulphur towards the electrophilic carbene carbon attached in an α-position as displayed by resonance structure **B** (Fig. 4). The α heteroatom substituent can potentially also act as an π-electron donor *via* its lone pair towards the electron withdrawing carbene carbon as shown in resonance structure **C**.

Significant shorter bond distances (Å) for both C_{carb}–C_{ipso}(Ar) (1.443(4) **1**, 1.456(3) **2**) and Co–C_{carb} (1.913(3) **1**, 1.922(2) **2**) of the ethoxycarbene complexes compared to the corresponding distances in the aminocarbene complexes, **4, 5** are recorded. For optimum electronic interaction the metal, heteroatom, the carbene carbon and the *ipso* carbon of the aryl substituent should be close to planar. The torsion angle representing rotation around the Co–C_{carb}–$X_{O/N}$–C_{het} (where C_{het} = methylene carbon of OEt, or methyl of NMe_2) deviates with less than 7° for all complexes. If one considers the planes P2 (Co–C_{carb}–$X_{O/N}$) and P3 (Co–C_{carb}–C_{ipso}), the relative distance of C_{ipso} with P2, as well as $X_{O/N}$ with P3 may help to qualitatively compare the distortion from the ideal planar conformation where all of the atoms Co, C_{carb}, $X_{O/N}$, and C_{ipso} lie in the same plane. From Table 3 only slight distortions are evident with the maximum observed for **6** with 0.072 Å (C_{ipso} from P2). The rotation around the C_{carb}–C_{ipso}(Ar) bond (X–C_{carb}–C_{ipso}–C_{Ar}) is informative and describes the rotation or tilting of the aromatic ring and is the major contributor of relieving steric congestion. The latter shows smaller angles for the ethoxycarbene complexes to maximize electronic effects of the aryl substituents and greater rotation values for the aminocarbene complexes to optimize the electronic effects of the aminocarbene substituent. The electronic favoured position for the aminocarbene substituent is in the plane of the carbene carbon forcing the aryl rings to tilt and take up sterically favoured positions. For the thienyl substituent this places the thienyl π-system out of phase with the empty p-orbital of the carbene carbon atom and nitrogen lone pair. The amino substituent, which is the stronger π-donor, dominates and emphasizes the important contribution of the resonance structure **C** in the aminocarbene complexes. Conclusions drawn from the changes in chemical shifts of **1**–**6** of NMR solution data are supported by the data obtained from solid state single crystal structure determinations. By example, bond lengths of the thienyl substituent in the ethoxycarbene complex **1** and the corresponding aminocarbene complex **4** are summarised in Fig. 7. A similar figure for the ethoxycarbene (**2**) and aminocarbene (**5**) complexes of DMA can be found in the ESI (Fig. S16).

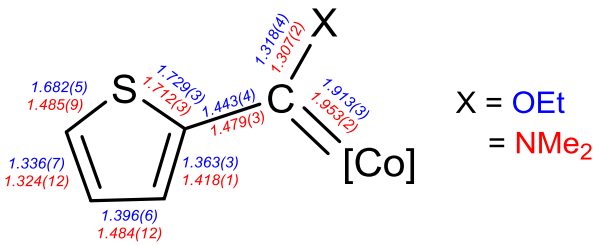

Fig. 7. Comparison of relevant bond lengths (Å) between the thienylcarbene ligand of **1** (*X*=OEt) and **4** (*X*=NMe_2).

3. Conclusions

The FCCs **1**–**6** display a trigonal bipyramidal molecular structure, consisting of an equatorial plane of three carbonyl ligands and a bulky triphenyl-tin group in an axial position that anchors the carbene ligand in the remaining axial position. The trigonal $Co(CO)_3$ plane forms a very stable core in the complex with strongly bonded, unreactive carbonyl ligands, in contrast to readily displaceable and modifying carbene ligands in the axial positions. In addition, the bulky $SnPh_3$ ligand in an axial position adds to the stability by blocking of one side of the molecule in the precursor [$Co(CO)_4SnPh_3$]. The remaining carbonyl, the most reactive site, is prone to nucleophilic attack by organolithium agents and, after subsequent alkylation, the neutral Co(I) complex, [$Co(CO)_3SPh_3${C(XŔ)}*R*], is generated. In this study, valuable information of the features and unique properties of the *R* substituents in the complexes are recognised for stability of the FCC of cobalt(I). For thiophene, the electron excessive nature and electron donating properties of the thienyl ring substituentare essential for electron density transfer by π-resonance effects in the ethoxycarbene complex. The use of a strong donating, remote dimethylamino substituent (NMe_2) in *p*-DMA to transfer electron density *via* the benzene ring towards the carbene carbon in ethoxycarbene complexes proved efficient. The tilting of the benzene ring due to steric constraints in the aminocarbene complexes diminishes the electron transfer process. Once aminolised, the tuneable electron density transfer role of the remote nitrogen unit (DMA) becomes redundant and is sacrificed to the more effective adjacent aminocarbene substituent. In the ferrocenyl carbene complex the negative charge of the bonded cyclopentadienyl fragment also accounts for a strong electron donor carbene substituent comparable to thienyl and DMA.

4. Experimental

4.1. General

All operations were carried out using standard Schlenk techniques or vacuum line techniques under an inert atmosphere of nitrogen or argon. Triethyloxonium tetrafluoroborate was prepared according to the method by Meerwein [32]. $Co_2(CO)_8$, *n*- and *tert*–butyllithium, thiophene, ferrocene and 4-bromodimethylaniline were purchased from Sigma Aldrich or Strem Chemicals and used as received. $Co(CO)_4SnPh_3$ was prepared according to the method by Curtis [31]. Anhydrous THF (tetrahydrofuran) and hexane were dried over sodium metal and DCM (dichloromethane) over CaH_2. Chromatography separations were also carried out under an inert atmosphere using silica gel 60 (particle size 0.063–0.20 mm) as resin.

4.2. Characterization and analytical techniques

4.2.1. Nuclear magnetic resonance spectroscopy

The recording of NMR spectra was done on a Bruker AVANCE 500, Ultrashield Plus 400 AVANCE 3 and Ultrashield 300 AVANCE 3 spectrometers, at 25 °C. Recording of the ^{1}H NMR spectra was done at 500.139, 400.13 or 300.13 MHz, and the ^{13}C NMR spectra at 125.75, 100.613 or 75.468 MHz. Deuterated chloroform ($CDCl_3$) signal was referenced to 7.26 ppm for δ_H and 77.00 ppm for δ_C.

4.2.2. Fourier-transform infrared spectroscopy

Infrared spectroscopy was recorded on a Bruker ALPHA FT-IR spectrophotometer with a NaCl cell. Hexane was used as solvent. The IR data are reported in the format: absorption intensity (assignment) in the order of highest to lowest wavenumber. The wave intensities are: *vw* – very weak, *w* – weak, *m* – medium, *s* –strong, *vs* – very strong, *sh* – shoulder and *br* – broad.

4.2.3. High-resolution mass spectrometry

Mass spectral analyses for **2** and **6** were performed on a Waters® Synapt G2 high definition mass spectrometer (HDMS) that consists of a Waters Acquity Ultra Performance Liquid Chromatography (UPLC®) system hyphenated to a quadrupole-time-of-flight (QTOF) instrument. Data acquisition and processing was carried out with MassLynxTM (version 4.1) software.

4.2.4. X-ray diffraction analysis

Single crystal diffraction data for **1, 2, 4–6** were collected at 150 K on a Bruker D8 Venture diffractometer with a kappa geometry goniometer and a Photon 100 CMOS detector using a Mo-Kα IμS.micro focus source. Data were reduced and scaled using SAINT and absorption intensity corrections were performed using SADABS (APEX III control software) [44]. X-ray diffraction measurements were performed at 293 K using an Oxford Cryogenics Cryostat. All structures were solved by an intrinsic phasing algorithm using SHELXTS [45] and were refined by full-matrix least-squares methods based on F^2 using SHELXL [46]. All non-hydrogen atoms were refined anisotropically. All hydrogen atoms were placed in idealized positions and refined using riding models. The crystal data collection and structure refinement parameters are provided in the Supplementary Material.

4.3. Synthesis and characterisation of ethoxycarbene complexes

4.3.1. Synthesis of complex **1** *[Co(CO)$_3$SnPh$_3${C(OEt)(C$_4$H$_3$S)}]*

A solution of *n*-BuLi (3.1 mL, 4.5 mmol) was added dropwise to the solution of thiophene (0.36 g, 4.5 mmol) in 80 mL THF at –10 °C while stirring vigorously. The turbid solution was stirred for 30 min at room temperature and then lowered to –78 °C. 1.57 g (3.0 mmol) of solid $Co(CO)_4SnPh_3$ was gradually added while vigorously stirring. Stirring was continued for an hour at –78 °C and the solution temperature was slowly raised to room temperature over an hour and left there for another hour with continuous vigorous stirring for the reaction to go to completion. The solvents were then removed from the resultant dark brownish solution under reduced pressure and the dark residue left was dissolved in 20 mL DCM and alkylated with 0.86 g (4.5 mmol) of $[Et_3O]$ $[BF_4]$ at –60 °C. After 30 min, the temperature of the solution was raised to room temperature and further stirring was applied for an hour followed by filtration on ($MgSO_4$ (dried): silica gel) resin with DCM as an eluent. The solvents were then removed under reduced pressure and the dark residue was purified through a column of hexane: DCM (5:1) and afforded a light orange product **1**. Yield: 0.43 g, 0.67 mmol, 22%.

Yield: 0.43 g (0.67 mmol, 22%), orange crystals. **FT-IR:** υ_{CO}(hexane)/cm^{-1} 2033 ($A_1^{(1)}$), 1955 (E). **^{1}H NMR:** δ^{1}H (300.13 MHz; $CDCl_3$; Me_4Si) 8.31 (dd, 1 H, $^{3}J_{3,4}$ = 4.0 Hz, $^{4}J_{3,5}$ = 1.0 Hz, H3), 7.83 (dd, 1H, $^{3}J_{5,4}$ = 4.0 Hz, $^{4}J_{5,3}$ = 1.0 Hz, H5), 7.67 (m, 6H, H2″o), 7.37 (m, 6H, H3″m), 7.35 (m, 3H, H4″p), 7.20 (dd, 1 H, $^{3}J_{4,5}$ = 4.9, $^{3}J_{4,3}$ = 4.1 Hz, H4), 5.07 (2 H, q, 3J = 7.1, CH_2), 1.69 (3 H, t, 3J = 7.1, CH_3). **^{13}C NMR:** δ^{13}C (75.468 MHz; $CDCl_3$; Me_4Si) 297.0 (C1), 200.7 (CO), 154.7 (C2), 140.8 (C3), 137.0 (C5), 136.5 (C2″), 129.0 (C4), 129.0 (C4″), 128.3 (C3″), 142.1 (C1″), 77.7 (CH_2), 14.7 (CH_3).

4.3.2. Synthesis of complex **2** *[Co(CO)$_3$SnPh$_3${C(OEt)(C$_8$H$_{10}$N)}]*

A solution of *n*-BuLi (3.1 mL, 4.5 mmol) was slowly added dropwise to a solution of 4-bromodimethylaniline (0.90 g, 4.5 mmol) in 25 mL diethylether at –10 °C while vigorously stirring and thereafter the temperature was allowed for 30 min to rise to room temperature. 1.57 g (3.0 mmol) of $Co(CO)_4SnPh_3$ in 25 mL diethyl ether was slowly added *via* a cannula to the solution of the lithiated dimethylaniline at –78 °C while vigorously stirring. After 30 min the temperature was allowed to rise to room temperature over a period of an hour while vigorously stirring. The solvents were then removed from the resultant dark brownish solution under reduced pressure and the dark residue left was dissolved in 20 mL DCM and alkylated with 0.86 g (4.5 mmol) of $[Et_3O]$ $[BF_4]$ at –60 °C. After 15 min, the temperature of the solution was raised to room temperature and further stirring was applied for an hour followed by filtration on ($MgSO_4$ *(dried)*: silica gel) resin with DCM eluent. The solvents were then removed *in vacuo* and the dark residue was purified through a hexane: DCM (5:1) column and afforded an orange-reddish product **2**. Yield: 1.32 g, 2.0 mmol, 65%.

2: Yield: 1.32 g (2.0 mmol, 65%), orange-reddish crystals. **FT-IR:** υ_{CO}(hexane)/cm^{-1} 1947 (E). **^{1}H NMR:** δ^{1}H (300.13 MHz; $CDCl_3$; Me_4Si) 7.97 (d, 2H, $^{3}J_{3,4}$ = 8.8 Hz, H3), 7.68 (m, 6H, H2″o), 7.35 (m, 6H, H3″m), 7.35 (m, 3H, H4″p), 6.61 (d, 2 H, $^{3}J_{3,4}$ = 0.8.9 Hz, H4), 5.07 (q, 2 H, 3J = 6.9 Hz, CH_2), 3.11 (s, 6H), 1.68 (t, 3H, 3J = 7.0 Hz, CH_3). **^{13}C NMR:** δ^{13}C (75.468 MHz; $CDCl_3$; Me_4Si) 304.1 (C1), 200.8 (CO), 154.2 (C2), 142.9 (C1″), 139.4 (C5), 136.7 (C2″), 132.9 (C3), 129.1 (C4″), 128.1 (C3″), 110.0 (C4), 77.7 (CH_2), 40.1 (2 x CH_3), 14.9 (CH_3). **HR-MS:** ESI-MS (positive mode, *m/z*): calcd for 672.0601; found 672,0625 (100%, $[M+H]^+$), calcd for 671.0529; found 671.0645 (45%, $[M]^+$), 643.0680 (13%, $[M–CO]^+$), 615.0149 (3%, $[M–2CO]^+$), 587.0807 (34%, $[M–3CO]^+$)

4.3.3. Synthesis of complex **3** *[Co(CO)$_3$SnPh$_3${C(OEt)(C$_{10}$H$_9$Fe}]*

Similar reaction procedure as in the synthesis of **5** was followed. 0.84 g (4.5 mmol) of ferrrocene in 100 mL THF was lithiated with 2.6 mL (4.5 mmol) of *tert*–BuLi at –78 °C, followed by reaction with 1.48 g (3.0 mmol) of $[(C_6H_5)_3SnCo(CO)_4]$ at –78 °C and alkylation with 0.86 g (4.5 mmol) of $[Et_3O]$ $[BF_4]$ at –60 °C respectively. Subsequent column purification, a light red product **3** was isolated and characterized. Yield: 0.19 g, 0.26 mmol, 9%.

3: Yield: 0.19 g (0.26 mmol, 9%), red crystals. **FT-IR:** υ_{CO}(hexane)/cm^{-1} 2016 ($A_1^{(1)}$), 1944 (E). **^{1}H NMR:** δ^{1}H (300.13 MHz; $CDCl_3$; Me_4Si) 7.67 (m, 6H, H2″o), 7.37 (m, 6H, H3″m), 7.35 (m, 3H, H4″p) 5.10 (2H, s, br, H3), 4.97 (2 H, q, 3J = 7.1 Hz, CH_2), 4.81 (2H, s, br, H4), 4.26 (5H, s, H5), 1.64 (3 H, t, 3J = 7.1 Hz, CH_3). **^{13}C NMR:** δ^{13}C (75.468 MHz; $CDCl_3$; Me_4Si) 309.5 (C1), 201.1 (CO), 142.5 (C1″), 136.6 (C2″), 129.1 (C4″), 128.2 (C3″), 77.7 (CH_2), 74.7 (C2), 72.7 (C3), 70.9 (C5), 69.7 (C4), 14.9 (CH_3).

4.4. Aminolysis of the ethoxycarbene complexes

4.4.1. Synthesis of complex **4** *[Co(CO)$_3$SnPh$_3${C(NMe$_2$)(C$_4$H$_3$S)}]*

Ethoxycarbene complex **1** (0.32 g, 0.50 mmol) was initially dissolved in 10 mL THF. To the reaction mixture, dimethylamine hydrochloride (0.049 g, 0.60 mmol) and sodium hydroxide (0.024 g, 0.60 mmol) were added while vigorously stirring. Degassed distilled water was then added dropwise until the pale yellow colour

was observed. The reaction was further stirred for 20 min for the reaction to go to completion. Progress throughout the reaction was followed with a TLC until all the starting material has reacted. Two layers were observed and the organic phase was washed with dried diethyether and filtered over ($MgSO_4$ *(dried)*: silica gel) resin. Solvents were removed under reduced pressure and after column chromatography purification with a mixture of hexane: diethylether (8:2), yellow complex **4** was obtained in good yields. Yield: 0.22 g, 0.34 mmol, 68%.

4: Yield: 0.22 g, (0.34 mmol, 68%), yellow crystals. **FT-IR:** υ_{CO}(hexane)/cm^{-1} 1992 (A_1), 1942 (E). **^{1}H NMR:** δ^1H(300.13 MHz; $CDCl_3$; Me_4Si) 7.61 (m, 6H, H2″o), 7.33 (1 H, dd, br, H3), 7.32 (m, 6H, H3″m), 7.30 (m, 3H, H2″p), 7.00 (1H, dd, $^3J_{4,3} = 5.0$, $^3J_{4,5}$ 3.5, H4), 6.64 (1H, dd, $^3J_{5,4} = 3.5$, $^4J_{5,3}$ 1.1, H5), 4.00 (3H, s, CH_3), 3.34 (3H, s, CH_3). **^{13}C NMR:** δ^{13}C(75.468 MHz; $CDCl_3$; Me_4Si) 252.2 (C1), 200.0 (CO), 152.0 (C2), 143.1 (C1″), 136.5 (C2″), 128.1 (C4″), 128.0 (C3″), 127.0 (C3), 124.9 (C5), 119.8 (C4), 51.1 (CH_3), 45.9 (CH_3).

*4.4.2. Synthesis of complex **5** [$Co(CO)_3SnPh_3\{C(NMe_2)(C_8H_{10}N)\}$]*

Ethoxycarbene complex **2** (0.67 g, 1.0 mmol) was initially dissolved in 10 mL THF. To the reaction mixture, dimethylamine hydrochloride (0.098 g, 1.2 mmol) and sodium hydroxide (0.048 g, 1.2 mmol) were added while vigorously stirring. Degassed distilled water was then added dropwise to the solution until the yellow colour was observed. Similar to complex **4**, the reaction progress was monitored with a TLC until all the starting material has reacted. Two layers were observed and the organic phase was washed with dried diethylether and filtered over ($MgSO_4$ *(dried)*: silica gel) resin. Solvents were removed *in vacuo* and column chromatography with a mixture of hexane: diethylether (8:2) afforded yellow complex **5** in good yields: 0.44 g, 0.66 mmol, 66%.

5: Yield: 0.44 g (0.66 mmol, 66%), yellow crystals. **FT-IR:** υ_{CO}(hexane)/cm^{-1} 2016 ($A_1^{(1)}$), 1937 (E). **^{1}H NMR:** δ^1H(300.13 MHz; $CDCl_3$; Me_4Si) 7.62 (br, 6H, H2″o)), 7.30 (br, 6H+3H, H3″m and H4″p) 6.80 (d, 2H, $^3J_{3,4} = 0.8.7$ Hz, H3), 6.70 (d, 2H, $^3J_{4,3} = 8.7$ Hz, H4), 3.97 (s, 3H, CH_3), 3.22 (s, 3H, CH_3), 2.97 (s, 6H, CH_3). **^{13}C NMR:** δ^{13}C(75.468 MHz; $CDCl_3$; Me_4Si) 257.9 (C1), 200.3 (CO), 148.9 (C2), 143.6 (C1″), 141.5 (C5), 136.6 (C2″), 127.9 (C4″), 127.9 (C3″), 122.1 (C3), 111.5 (C4), 50.6 (CH_3), 45.3 (CH_3), 40.2 (CH_3).

*4.4.3. Aminolysis of **2** to form **6**, [$Co(CO)_3SnPh_3\{C(NHCH_2CH_2NMe_2)(C_8H_{10}N)\}$]*

(0.32 g, 0.5 mmol) of ethoxycarbene complex **7** was initially dissolved in a mixed solution of hexane / THF (10:1). To the reaction mixture, 1,1-dimethylethylenediamine (0.055 mL, 0.5 mmol) was added while vigorously stirring. The colour immediately changed from orange to light brown. The mixture was then immediately subjected to irradiation for 2 h. After irradiation, the mixture was allowed to cool down and the reaction was tested with a TLC for completion. Solvents were then removed under reduced pressure and the brown residue washed with diethylether afforded the light brown aminocarbene complex **6**. Yield: (0.15 g, 0.21 mmol, 42%).

6: Yield: 0.15 g (0.21 mmol, 42%), yellow crystals. **FT-IR:** υ_{CO}(hexane)/cm^{-1} 2012 ($A_1^{(1)}$), 1939 (E). **^{1}H NMR:** δ^1H(300 MHz; $CDCl_3$; Me_4Si) 9.59 (1H, s, br, H1), 7.65 (m, 6H, H2″o), 7.33 (6H, m, H3″m), 7.29 (3H, m, H4″m), 7.11 (2H, d, $^3J_{3,4} = 8.8$, H3), 6.70 (2H, d, $^3J_{4,3} = 8.8$, H4), 3.44 (2H, dd, $3J = 11.3$, $3J = 5.4$, CH_2), 2.47 (2H, t, $3J = 11.7$, $3J = 5.7$ Hz CH_2), 3.02 (3H, s, CH_3), 2.30 (3H, s, CH_3), **^{13}C NMR:** δ^{13}C(75.468 MHz; $CDCl_3$; Me_4Si) 258.5 (C1), 201.7 (CO), 150.3 (C2), 143.8 (C1″), 136.7 (C2″), 136.1 (C5), 127.9 (C4″), 127.9 (C3″), 125.2 (C3), 110.9 (C4), 57.2 (CH_2), 47.7 (CH_2), 45.1 (2 x CH_3), 40.2 (2 x CH_3). **HR-MS:** ESI-MS (positive mode, *m/z*): calcd for 714.1183; found 714.1056 (26%, $[M+H]^+$), calcd for 713.1111; found 713.1066 (53%, $[M]^+$), 685.1114 (100%, $[M–CO]^+$), 657.1168 (52%, $[M–2CO]^+$), 629.1211 (3%, $[M–3CO]^+$).

4.5. Reaction of ***6*** by (i) reflux and (ii) irradiation

(i) A THF solution of **6** was refluxed for 5 h.
(ii) A solution of **6** dissolved in 10 ml THF and 100 mL hexane was added and the solution irradiated for 2 h.

In both cases (i) and (ii) above, the yellow reaction mixture turned brown and excessive decomposition occurred. TLC revealed no new coloured product and all of **6** was consumed.

Declaration of Competing Interest

The authors declare the following financial interests/personal relationships which may be considered as potential competing interests: Daniela I. Bezuidenhout reports financial support was provided by National Research Foundation, South Africa. Daniela I. Bezuidenhout reports financial support was provided by Sasol Technology R&D Pty. Ltd.

CRediT authorship contribution statement

Mmushi M. Moeng: Investigation, Validation, Data curation, Writing – original draft. **Frederick P. Malan:** Investigation, Writing – review & editing. **Simon Lotz:** Conceptualization, Formal analysis, Supervision, Writing – original draft, Writing – review & editing. **Daniela I. Bezuidenhout:** Conceptualization, Validation, Supervision, Writing – original draft, Writing – review & editing.

Acknowledgements

The authors gratefully acknowledge the National Research Foundation, South Africa [NRF 105740; NRF 105529 NRF 87788 and NRF 9772] and Sasol Technology R&D Pty. Ltd. (South Africa) for financial support.

Supplementary materials

Supplementary material associated with this article can be found, in the online version, at doi:10.1016/j.molstruc.2021.132093.

References

[1] L.J. Taylor, D.L. Kays, *Dalton Trans.* 48 (2019) 12365.
[2] J. Cheng, L. Wang, P. Wang, L. Deng, Chem. Rev. 118 (2018) 9930.
[3] V. Charra, P. de Frémont, P. Braunstein, Coord. Chem. Rev. 341 (2017) 53.
[4] S. Díez-González, N. Marion, S.P. Nolan, Chem. Rev. 109 (2009) 3612.
[5] E.O. Fischer, A. Maasböl, Angew. Chem. 76 (1964) 645.
[6] G.K. Ramollo, I. Strydom, M.A. Fernandes, A. Lemmerer, S.O. Ojwach, J.L. van Wyk, D.I. Bezuidenhout, Inorg. Chem. 59 (2020) 4810.
[7] T.L. Mashabane, G.K. Ramollo, G. Kleinhans, S. de Doncker, S. Siangwata, M.A. Fernandes, A. Lemmerer, G.S. Smith, D.I. Bezuidenhout, J. Organomet. Chem. 690 (2020) 121341.
[8] G.K. Ramollo, M.J. López-Gómez, D.C. Liles, L.C. Matsinha, G.S. Smith, D.I. Bezuidenhout, *Organometallics* 34 (2015) 5745.
[9] D.J. Darensbourg, M.Y. Darensbourg, Inorg. Chem. 9 (1970) 1691.
[10] F. Carre, G. Cerveau, E. Colomer, R.J.P. Corriu, J.C. Young, J. Organomet. Chem. 179 (1979) 215.
[11] G. Cerveau, E. Colomer, R.J.P. Corriu, J.C. Young, J. Organomet. Chem. 205 (1981) 31.
[12] W.D. Wulff, S.R. Gilbertson, J.P. Springer, J. Am. Chem. Soc. 108 (1986) 520.
[13] A.C. Filippou, E. Herdtweck, H.G. Alt, J. Organomet. Chem. 355 (1988) 437.
[14] E.O. Fischer, V. Kiene, J. Organomet. Chem. 23 (1970) 215.
[15] M.F. Semmelhack, R. Tamura, J. Am. Chem. Soc. 105 (1983) 4099.
[16] C. Jiabi, L. Guixin, X. Weihua, J. Organomet. Chem. 286 (1985) 55.
[17] S. Lotz, P.H. van Rooyen, M.M. van Dyk, *Organometallics* 6 (1987) 499 ib>.
[18] S. Lotz, J.L.M. Dillen, M.M. van Dyk, J. Organomet. Chem. 371 (1989) 371.
[19] B. van der Westhuizen, P.J. Swarts, I. Strydom, D.C. Liles, I. Fernández, J.C. Swarts, D.I. Bezuidenhout, Dalton Trans. 42 (2013) 5367.
[20] J.A. Connor, J.P. Lloyd, J. Chem. Soc., Dalton Trans 14 (1972) 1470.
[21] R. Metelkova, T. Tobrman, H. Kvapilova, I. Hoskovcova, J. Ludvik, Electrochim. Acta 82 (2012) 470.
[22] S. Lotz, M. van den Berg, J.L. Dillen, Trans. Met. Chem. 13 (1988) 170.
[23] N.-A. Weststrate, C. Hassenrück, M. Linseis, D.C. Liles, S. Lotz, H. Görls, R.F. Winter, Z. Allg. Anorg. Chem. 67 (2021) 1152.

[24] N.-A. Weststrate, C. Hassenrück, D.C. Liles, S. Lotz, H. Görls, R.F. Winter, J. Organomet. Chem. (2021) 954–955 122113.
[25] L.F.C. de la Cruz, M.C. Ortega-Alfaro, J.G. Lopez-Cortez, R.A. Toscano, C. Alvarez–Toledano, H. Rudler, J. Organomet. Chem. 690 (2005) 2229.
[26] H.G. Raubenheimer, S. Cronje, Dalton Trans. (2008) 1265.
[27] M.F. Semmelhack, A. Chlenov, Top. Organomet. Chem. 7 (2004) 21.
[28] R.J. Card, W.S. Trahanovsky, J. Org. Chem. 45 (1980) 2560.
[29] A.R. Lepley, W.A. Khan, A.B. Giumanini, A.G. Giumanini, J. Org. Chem. 31 (1966) 2047.
[30] B. Bildstein, M. Malaun, H. Kopacka, K. Wurst, M. Mitterböck, K.-H. Ongania, G. Opromolla, P. Zanello, *Organometallics* 18 (1999) 4325.
[31] M.D. Curtis, Inorg. Chem. 11 (1972) 802.
[32] H. Meerwein, Org. Synth. 46 (1966) 113.
[33] Z. Lamprecht, S.G. Radhakrishnan, A. Hildebrandt, H. Lang, D.C. Liles, N. Westrate, S. Lotz, D.I. Bezuidenhout, Dalton Trans 46 (2017) 13983.
[34] D.I. Bezuidenhout, S. Lotz, M. Landman, D.C. Liles, Inorg. Chem. 50 (2011) 1521.
[35] D. Munz, *Organometallics* 37 (2018) 275.
[36] H.G. Raubenheimer, *Dalton Trans.* 43 (2014) 16959.
[37] D.M. Andrada, M.E. Zoloff Michoff, I. Fernández, A.M. Granados, M.A. Sierra, *Organometallics* 26 (2007) 5854.
[38] I. Fernández, F.P. Cossio, A. Arrieta, B. Lecea, M.J. Mancheño, M.A. Sierra, *Organometallics* 23 (2006) 1065.
[39] D.A. Valyaev, R. Brousses, N. Lugan, I. Fernández, M.A. Sierra, Chem. Eur. J. 17 (2011) 6602.
[40] M. Landman, H. Görls, S. Lotz, Z. Anorg, Allg. Chem. 628 (2002) 2037.
[41] Y.M. Terblans, S. Lotz, *S. J. Chem, Soc., Dalton Trans.* (1997) 2177.
[42] M. Landman, H. Görls, S. Lotz, Eur. J. Inorg. Chem. (2001) 233.
[43] B.Y.K. Ho, Y. Zuckerman, J. Organomet. Chem. 49 (1973) 1.
[44] APEX3. (including SAINT and SADABS), BrukerAXS Inc., Madison, WI, 2016.
[45] G.M. Sheldrick, Acta Crystallogr. Sect. A Found. Adv. 71 (2015) 3.
[46] G.M. Sheldrick, Acta Crystallogr. Sect. C Struct. Chem. 71 (2015) 3.